## EXTENDED EXPERIMENTAL PROCEDURES

### Plasmids

Plasmids expressing GFP tagged proteins were obtained by insertion of PCR-amplified coding regions of cDNAs from the *Drosophila* Genomic Resource Center (DGRC). All PCR products were cloned into AscI/PacI digested pCopia-LAP-EGFP plasmid (described in Cheeseman and Desai, 2005) except for Smc6, which was cloned into KpnI/NotI digested pMT-EGFP plasmid. pCopia-LAP-EGFP-PCNA and pMT-EGFP were kindly provided by B. Mellone. Plasmids expressing mCherry-tagged proteins were obtained by substituting EGFP in the pCopia-LAP-EGFP plasmid with mCherry using Nhe1/Xho1, then cloning the proper PCR products with AscI/PacI restriction sites. FLAG-HP1a (pCopia-3XFLAG-StrepII-myc-HP1a) was prepared by substituting EGFP-StrepII with 3XFLAG and StrepII-myc into pCopia-LAP-EGFP. Templates were: Rad51/SpnA (clone RH24133), Mdc1/Mu2 (clone LD44171), TopBP1/Mus101 (clone RE28166), ATRIP/Mus304 (clone LD44887), Smc5 (clone RE65864), Smc6 (clone SD25546), HP1a/Su (var)205 (clone LD10408). Detailed information about the DGRC clones can be found on Flybase (flybase.org). The sequence codifying for Nse2/Qjt was amplified from genomic DNA isolated from wild-type flies.

### Preparation of Cell Lines Expressing Tagged Proteins

Stable lines were obtained by selecting for expression of the pCopia plasmids with 500 μg/ml G418 (EMD), or by cotransfecting with the plasmid pCoHygro (Invitrogen) and selecting in the presence of 100 μg/ml hygromycin B (Invitrogen). Transfection was performed with DOTAP (Roche), according to manufacturer's procedures.

### Analysis of Tagged Proteins

We confirmed that the foci of Mu2, ATRIP, TopBP1 and Rad51, observed in time-lapse analysis of irradiated cells, correspond to DSB sites by performing IF with anti-γH2Av antibodies on fixed samples. GFP-Mu2 foci (as in Dronamraju and Mason, 2009), mCh-TopBP1 and GFP-Rad51 foci colocalized with γH2Av foci (data not shown). Colocalization of GFP-ATRIP and γH2Av foci is shown in Figure 1D. We also confirmed that GFP-HP1a colocalizes with H3K9me2 and with H3K9me3 after fixation, before and after IR (data not shown).

### dsRNA Synthesis and RNAi Depletion

Amplicons used to make dsRNAs were: Smc5 (DRSC11849, corresponding to #1 in Figure S8E and BKN22081, corresponding to #2 in Figure S8E), Smc6 (DRSC25997, corresponding to #2 in Figure S8E), Rad51 (DRSC16812), Rad54 (DRSC24838 and BKN27487), Su(var)3-9 (DRSC16873), HP1a (DRSC03446), SetDB1 (DRSC28455), ATM (DRSC16060 and DRSC36931), ATR (DRSC20350 and DRSC38547), CtIP (DRSC29281), Tosca/Exo1 (DRSC03624), bw (DRSC04005). Sequences can be found on Flybase. When two amplicons are indicated, we combined equal amounts of both dsRNAs for better efficiency of protein depletion. For depletion of Smc5/6 in Figure 6 and S8C, S8D, S8F and S8G we combined dsRNAs from the amplicons: DRSC11849, BKN22081 and DRSC25997. dsRNA for Blm, Ku70 and Ku80 were previously described in Min et al. (2004). Oligo sequences for making dsRNA #1 for Smc6 were: 5′- taatacgactcactataggg AAACGGTTCTTGTGACGGAG and 5′-taatacgactcactataggg TCCTTGATTGATGCTGACCA (lower cases indicate the T7-polymerase binding sequence). dsRNA was prepared with the MegaSCRIPT T7 kit (Applied Biosystems) and transfected with DOTAP (Roche). Templates for PCR were obtained from the DGRC. dsRNA derived from the brown gene (*Bw*) was used as control. The time of incubation with dsRNAs was 4 days (Ku70 and Ku80), 5 days (HP1a, Rad51, Rad54, Smc5/6, ATM, ATR, Blm, Tosca/Exo1, CtIP), 8 days (Su(var)3-9, SetDB1), which was optimized to maximize depletion of the proteins (assayed by Western blotting and IF) without impacting the cell cycle (assayed by FACS analysis). For Su(var)3-9 and SetDB1, 8 days of depletion was required to see significant depletion of H3K9me2 and H3K9me3. When depletion required more than 5 days, dsRNA was added again after 4 days. For Figure 6E and 6F and S8E, Smc5/6 RNAi was for 6.5 days.

All kinetics resulting from RNAi depletion must be compared to cells treated with control dsRNAs since the γH2Av peak shifts from 10 min (Figure 1B) to 20-30 min after IR (e.g., Figure 1C) in RNAi controls.

### FACS Analysis

Exponentially growing cells were washed in PBS, fixed in 70% ethanol, washed in PBS and resuspended in Tris 50mM pH 7.5 with 1 mg/ml RNaseA. DNA was stained with 50 μg/ml propidium iodide and analyzed with FACScan (BD).

### Q-PCR

Total RNA was isolated from 1-2 × $10^5$ cells using Nucleospin RNA II kit (Macherey- Nagel), and used to generate single-stranded cDNA using a poly dT primer and Superscript Reverse Transcriptase III (Invitrogen). Specific transcripts were quantified using intron-spanning primers with Absolute Blue QPCR SYBR low ROX mix (Thermo) and 7500 Fast Real-Time PCR (Applied Biosystems). Changes in transcript levels were normalized to Act5C mRNA. Primer sequences were: AACGGAACAGGAAGACATGC and GCTCTAGCGGGTTGTAGATA for Tosca, GAAGTCATAGAGGAGAGTCC and GGTCTTGACTGTGCTATTGC for CtIP, TTCGCA AGTGCTGCGAGATTAC and TTCGCCTGCTGTCGTTTAAC for ATR, TCAGTCGGTTTATTCCAGTC, CAGCAACTTCTTCGTCACACA for Atc5C.

### Western Blotting

$2 \times 10^6$ cells were harvested, washed once in PBS and lysed for 30 min in ice with RIPA buffer (50 mM Tris, pH8, 1% NP-40, 0.5% DOC, 0.1% SDS) containing protease inhibitors (Complete, Roche) and 1 mM PMSF. After centrifugation (14000 rpm, 20 min, 4°C) the supernatant was benzonase-treated for 1 hr at 4°C before adding Laemmli buffer to 1x and boiling for 3 min. Extracts were run in NuPAGE (Invitrogen) 4%–12% and 10% gels and transferred onto nitrocellulose membrane according to manufacturer's instructions.

### Antibodies

Antibodies used were: anti-Rad51 (kind gift from J. Kadonaga); anti-ATM, anti-Blm, anti-Ku70 and anti-Ku80 (kind gifts from D. Rio); anti-Lamin Dm0 and anti-HP1a (C1A9, used for WB and IF) (Hybridoma Bank); anti-SetDB1 and anti-HP1a (wa191, used for ChIP) (kind gifts from S. Elgin); anti-fibrillarin (Cytoskeleton, Inc.); anti-tubulin (Sigma-Aldrich); anti-H3K9me3, anti-H3K4me3, anti-H3K4me2, anti-Smc5, anti-Smc6 and anti-Okr (SDI); anti-γH2Av (Rockland); anti-H3K9me2 (Upstate); anti-GFP (Rockland); in Figure S5C anti-H3K9me3 was from Wako. Fluorescent and HRP-conjugated secondary antibodies were from Invitrogen. In Figure S4G, Cy5-conjugated secondary antibodies were from Jackson ImmunoResearch Laboratories.

### FISH Probes

AAGAG, AACAC, and dodeca FISH probes were made by end labeling of oligonucleotides with aminoallyl-dUTP (Sigma) followed by conjugation to Alexa-555 ester dyes (Invitrogen). The 359bp probe was made as described in Dernburg et al. (1996).

### Immunoprecipitation

For HP1a immunoprecipitation, $10^8$ S2 cells expressing, or lacking (control), FLAG-HP1a were incubated with lysis buffer (50 mM HEPES pH 7.6, 10 mM KCl, 2 mM MgCl2, 10% glycerol, 1 mM DTT, 0.5 mM EDTA, 25 mM NaF, 0.05% NP-40, 1 mM benzamidine, 1 mM PMSF, protease inhibitor cocktail (Roche) and digested with benzonase at 4°C for 30 min. Chromatin was extracted with 300 mM Na-acetate at 4°C for 30 min, and the lysate was cleared by centrifugation prior to incubation with FLAG M2 agarose beads (Sigma) for 2 hr. Beads were washed with lysis buffer and then heated in sample buffer for SDS-PAGE.

For ATRIP immunoprecipitation, $10^8$ Kc cells expressing GFP-ATRIP were pelleted and snap-frozen at different time points after IR. Pellets were lysed with lysis buffer + 20 mM 2-glycerophosphate. After isolating the soluble lysate by centrifugation, the pellet was resuspended in the same buffer, extracted with 300 mM sodium acetate for 1 hr at 4°C, and the supernatant was pooled with the soluble lysate. Half of each sample was incubated overnight at 4°C with 10-15 μl Protein G-coupled Sepharose beads and 3 μl of goat anti-GFP antibody, while the other half only received the beads as a negative control. The beads were then washed 3X with 50 mM HEPES, pH 7.6, 10mM KCl, 2 mM MgCl2, 0.05% NP-40, 150 mM sodium acetate. Samples were heated at 65°C for 5 min in sample buffer for SDS-PAGE.

### Cell Imaging in Time-Lapse Experiments

In time-lapse experiments, cells were imaged after settling on chambered coverglass slides (Thermo Scientific) for 10 min. A field of about 50 cells was imaged before IR and its XY coordinates were saved in softWoRX, allowing us to identify the same field after IR. Since Kc cells quickly adhere to the slides, their positions don't change during the IR and the imaging procedure, so there was virtually no cell drift between different time points.

### Quantitation of Heterochromatin Expansion

For quantifying the HP1a expansion in time-lapse experiments, 3D volumes occupied by HP1a were analyzed for consecutive time points in deconvolved time-lapse images of individual nuclei. Image manipulations and analysis were done with Matlab (MathWorks) and DIPimage (Image Processing Toolbox for Matlab, Delft University of Technology, The Netherlands). The HP1a domain was identified automatically using isodata thresholding (Ridler and Calvard, 1978) and confirmed manually. The volume of HP1a at each time point after IR was normalized to the volume (or mean volume) before IR for each cell.

For quantifying the DAPI- bright expansion, 3D volumes occupied by DAPI-bright were analyzed in samples fixed before and after IR. Image manipulations and analysis were done using Matlab (MathWorks). Nuclear segmentation was performed automatically with in-house algorithms (Costes et al., 2006; Costes et al., 2007) and DAPI-bright volumes were identified using a "tophat" filter followed by an interactive threshold, on a per nucleus basis. The volume of DAPI-bright was normalized to the nuclear volume (DAPI) for each cell.

For analysis of the distance between AACAC probes and DAPI-bright, AACAC repeats were localized by FISH in cells fixed before and after IR. The distance between AACAC signals and the surface of DAPI-bright was measured in 3D reconstructions of the nuclei with softWoRx and normalized to the nuclear diameter for each cell.

### NIR Treatment

NIR (Near-Infrared) laser experiments were performed using a multiphoton laser source coupled to a Zeiss 510 NLO Axiovert confocal microscope as described in Mari et al. (2006). Logarithmically growing Kc cells expressing HP1a-GFP were imaged to detect the position of heterochromatin before targeting with the laser, then fixed at the indicated time points before IF.

### Cell Treatments with Caffeine

15mM caffeine (stock 1.5M in water) was added to the culture for 60 min before IR.

### ChIP-Array

For each ChIP, chromatin from ~5x10$^7$ S2 cells were fixed and processed as described in www.modencode.org/protocols, using 15 μl anti-HP1a antibody. ChIP samples were amplified using the Genome Plex Complete WGA2 Kit (Sigma), fragmented to 50-100 bp by DNaseI, and labeled with biotin by TdT. Genomic DNA Tiling Arrays v1.0 (Affymetrix) were hybridized and imaged.

### SUPPLEMENTAL REFERENCES


Cheeseman, I.M., and Desai, A. (2005). A combined approach for the localization and tandem affinity purification of protein complexes from metazoans. Sci. STKE *2005*, pl1.

Cortez, D., Guntuku, S., Qin, J., and Elledge, S.J. (2001). ATR and ATRIP: partners in checkpoint signaling. Science *294*, 1713–1716.

Costes, S.V., Boissière, A., Ravani, S., Romano, R., Parvin, B., and Barcellos-Hoff, M.H. (2006). Imaging features that discriminate between foci induced by high- and low-LET radiation in human fibroblasts. Radiat. Res. *165*, 505–515.

Costes, S.V., Ponomarev, A., Chen, J.L., Nguyen, D., Cucinotta, F.A., and Barcellos-Hoff, M.H. (2007). Image-based modeling reveals dynamic redistribution of DNA damage into nuclear sub-domains. PLoS Comput. Biol. *3*, e155.

Dernburg, A.F., Broman, K.W., Fung, J.C., Marshall, W.F., Philips, J., Agard, D.A., and Sedat, J.W. (1996). Perturbation of nuclear architecture by long-distance chromosome interactions. Cell *85*, 745–759.

Dronamraju, R., and Mason, J.M. (2009). Recognition of double strand breaks by a mutator protein (MU2) in Drosophila melanogaster. PLoS Genet. *5*, e1000473.

Fischle, W., Tseng, B.S., Dormann, H.L., Ueberheide, B.M., Garcia, B.A., Shabanowitz, J., Hunt, D.F., Funabiki, H., and Allis, C.D. (2005). Regulation of HP1-chromatin binding by histone H3 methylation and phosphorylation. Nature *438*, 1116–1122.

Hirota, T., Lipp, J.J., Toh, B.H., and Peters, J.M. (2005). Histone H3 serine 10 phosphorylation by Aurora B causes HP1 dissociation from heterochromatin. Nature *438*, 1176–1180.

Kellum, R., Raff, J.W., and Alberts, B.M. (1995). Heterochromatin protein 1 distribution during development and during the cell cycle in Drosophila embryos. J. Cell Sci. *108*, 1407–1418.

Mari, P.O., Florea, B.I., Persengiev, S.P., Verkaik, N.S., Brüggenwirth, H.T., Modesti, M., Giglia-Mari, G., Bezstarosti, K., Demmers, J.A., Luider, T.M., et al. (2006). Dynamic assembly of end-joining complexes requires interaction between Ku70/80 and XRCC4. Proc. Natl. Acad. Sci. USA *103*, 18597–18602.

Min, B., Weinert, B.T., and Rio, D.C. (2004). Interplay between Drosophila Bloom's syndrome helicase and Ku autoantigen during nonhomologous end joining repair of P element-induced DNA breaks. Proc. Natl. Acad. Sci. USA *101*, 8906–8911.

Perrini, B., Piacentini, L., Fanti, L., Altieri, F., Chichiarelli, S., Berloco, M., Turano, C., Ferraro, A., and Pimpinelli, S. (2004). HP1 controls telomere capping, telomere elongation, and telomere silencing by two different mechanisms in Drosophila. Mol. Cell *15*, 467–476.

Ridler, T., and Calvard, S. (1978). Picture thresholding using an iterative selection method. IEEE Trans. Syst. Man Cybern. *SMC-8*, 630–632.

Sartori, A.A., Lukas, C., Coates, J., Mistrik, M., Fu, S., Bartek, J., Baer, R., Lukas, J., and Jackson, S.P. (2007). Human CtIP promotes DNA end resection. Nature *450*, 509–514.

Somanathan, S., Suchyna, T.M., Siegel, A.J., and Berezney, R. (2001). Targeting of PCNA to sites of DNA replication in the mammalian cell nucleus. J. Cell. Biochem. *81*, 56–67.

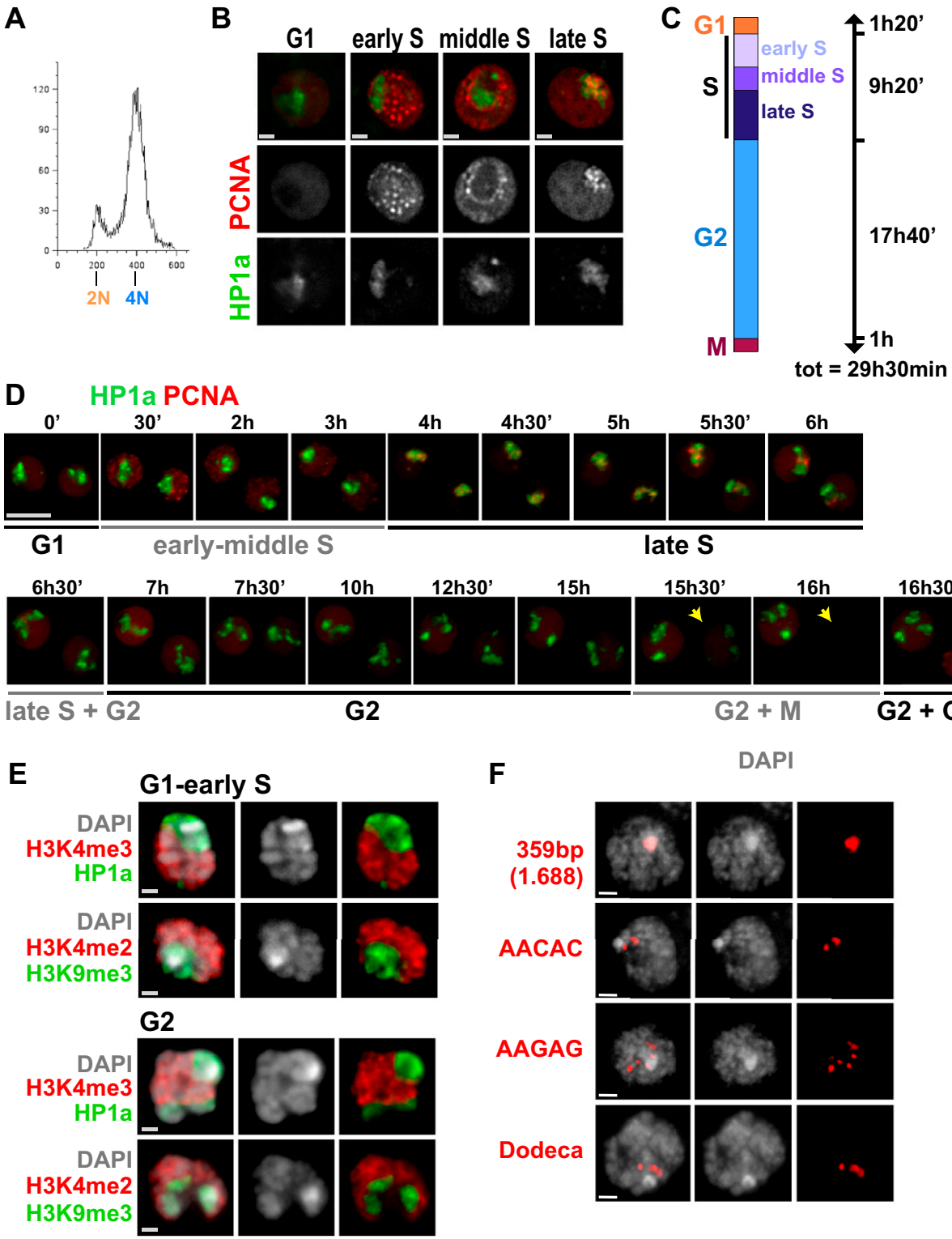


**Figure S1. Heterochromatin Occupies a Distinct Domain in *Drosophila* Cells in Different Cell-Cycle Phases, Related to Figure 1 and Figure 3**

The distributions of heterochromatin markers and repeated sequences were analyzed with respect to the DAPI-bright domain and the cell cycle in *Drosophila* Kc cells.

(A) FACS analysis of exponentially growing Kc cells shows that most of the cells have a 4N DNA content, consistent with G2.

(B) A cell line expressing GFP-HP1a and mCh-PCNA was used to analyze the progression of the cell cycle. PCNA is recruited to the replication forks during S phase. HP1a is associated with heterochromatin in interphase and disassembled in prophase (Fischle et al., 2005; Hirota et al., 2005; Kellum et al., 1995), thus HP1a disappearance was used to detect mitotic cells (an example is shown in D, arrow). Cells in mitosis were identified and imaged every 30 min for 24 hr. We observe that PCNA signal, which is diffuse in G1 nuclei, organizes in specific patterns reflecting the positions of the replication forks in S phase, similar to mammalian cells (Somanathan et al., 2001). In early S-phase, nuclei contain bright patches of PCNA, which then appear at the periphery of the nucleoli (middle-S), and finally overlap with HP1a (late-S). Scale bars = 1 μm.

(C) Quantitation of the cell cycle phases was obtained in time-lapse experiments by imaging cells expressing mCh-PCNA and GFP-HP1a every 30 min for 30 hr and calculating the average duration of each phase (n = 30). The pattern of PCNA during S-phase was used to monitor the G1-S, intra-S and S-G2 transitions, while disappearance of HP1a in M phase marked the G2-M and M-G1 transitions. This analysis revealed that the G1 phase is very short, while most Kc cells in culture are in late S or G2 phases, consistent with the FACS analysis (A).

(D) Representative time points from the experiment described in (C) revealed that the HP1a domain is single and compact from G1 to middle-S, and frequently splits into two or three sub-domains from late-S to G2. This multi-lobed organization of HP1a was never observed in G1 and early-S phase. Disassembly of the HP1a signal is observed in mitosis (M, arrow). Scale bar = 5 μm. Images are maximum intensity projections.

(E) Cells were fixed and immunostained with antibodies recognizing markers enriched in euchromatin (H3K4me2 or me3), heterochromatin (HP1a, H3K9me3), and DAPI. Images show that the DAPI-bright region is enriched for H3K9me3 and HP1a, and that H3K4me2 and me3 are excluded from regions containing heterochromatin markers. H3K9me2 staining is similar to H3K9me3 (not shown) and HP1a (shown in S3C). This distinct separation is visible in G1/S and G2 cells (identified by the multi-lobed shape of HP1a, see D). Scale bars = 1 μm. Images are maximum intensity projections of Z-stacks spanning the DAPI-bright region.

(F) FISH analysis of different satellite repeats in Kc cells shows that the 359-bp satellite, located on the X chromosome, is consistently located in DAPI-bright, some (AAGAG)n and (AACAC)n repeats are associated with DAPI-bright while others are not, and Dodeca is usually outside DAPI-bright. Thus, similar to heterochromatin marks, satellite repeats colocalize with and extend beyond the DAPI-bright region, Scale bars = 1 μm. Images are maximum intensity projections of the nucleus.

These analyses revealed that heterochromatin is organized in a distinct nuclear domain in *Drosophila* cells in interphase, and that DAPI-bright can be used as a conservative measure of the extent of the heterochromatic domain.

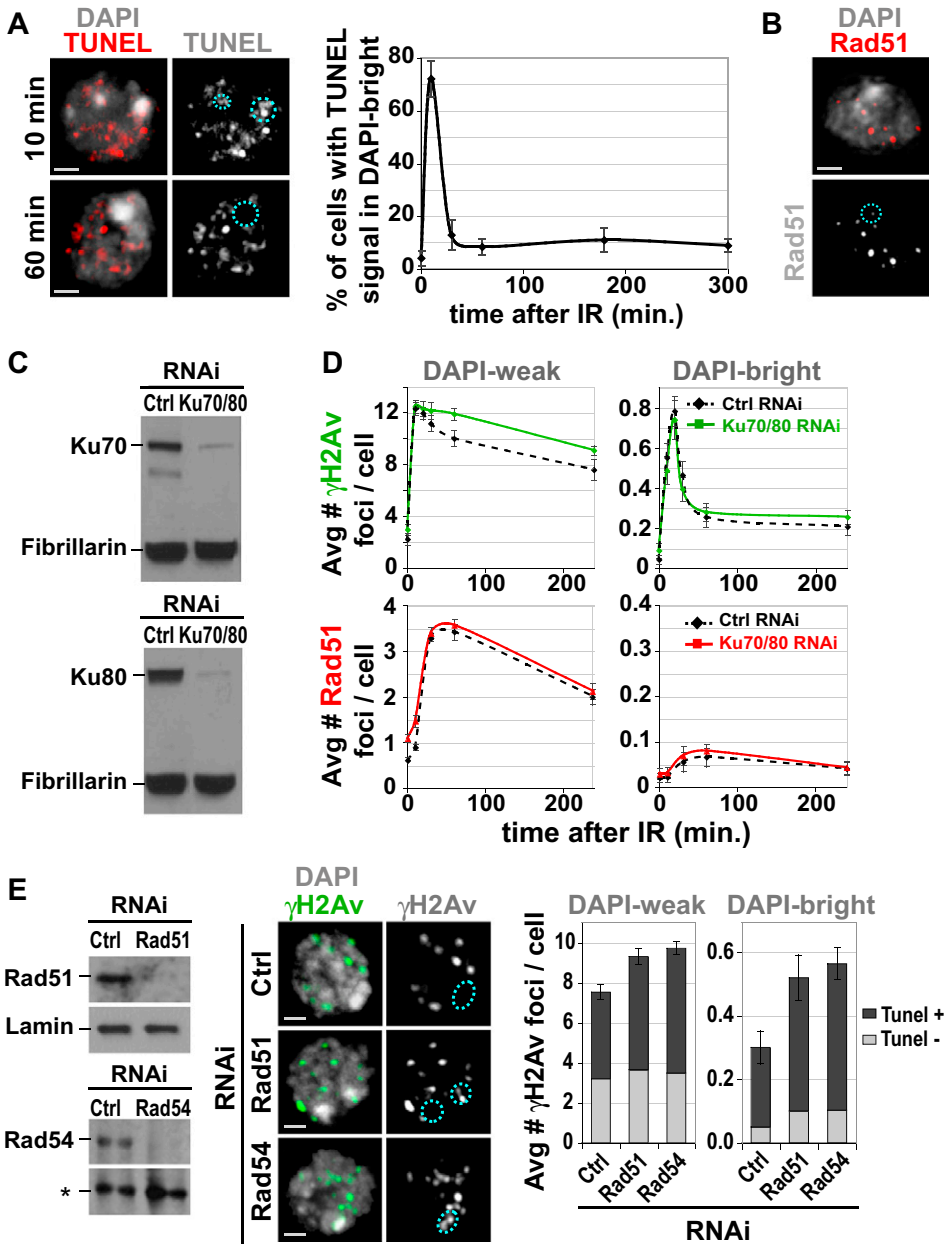


**Figure S2. Rad51 or Rad54 Depletion, and not Ku70/80 Depletion, Result in Persistent DSBs in Heterochromatin, Related to Figure 1**

(A) DNA breaks are formed in heterochromatin and quickly disappear. Cells were fixed at different time points after IR and stained using TUNEL (red) and DAPI. Representative images show signals in DAPI-bright at 10 min and not at 60 min (left). Quantitation (graph, right) shows that TUNEL signals peak at 10 min after IR in DAPI-bright; the % of cells is significantly different from untreated cells and subsequent time points ($p < 0.001$, $n > 100$).

(B) A cell from the experiment described in Figure 1A shows a rare example of a Rad51 focus assembled in DAPI-bright at 60 min after IR.

(C) Western analysis confirms nearly complete depletion of Ku70 and Ku80 after RNAi. Fibrillarin is the loading control.

(D) Ku70/80 depletion does not impact the kinetics of γH2Av foci in heterochromatin. After RNAi depletion of Ku70 and Ku80, cells were irradiated, fixed and stained with γH2Av or Rad51 antibodies. Top graphs shows that Ku70/80 removal results in increased γH2Av foci in euchromatin (DAPI-weak) ($p < 0.05$, $n > 100$), but not in heterochromatin (DAPI-bright). Bottom graphs show that Ku70/80 removal does not impact the kinetics of Rad51 foci appearance and disappearance in euchromatin (DAPI-weak) or in heterochromatin (DAPI-bright) ($n > 200$).

(E) Rad51 or Rad54 RNAi depletion results in persistent DSBs in heterochromatin. Left: Western blot analysis of extracts from cells used for the experiment described in Figure 1C confirm that Rad51 and Rad54 RNAi results in significant protein depletion, compared to control RNAi. Lamin and a non-specific band (*) are loading controls for Rad51 and Rad54, respectively. Center: Depletion of Rad51 or Rad54 results in retention of γH2Av foci (green) in DAPI-bright 60 min after IR, which is not observed in controls (see Figure 1C for kinetics). Right: after Rad51, Rad54 or control RNAi, cells were fixed 4h after IR, and stained for TUNEL and with anti-γH2Av antibodies. The histogram shows that about 80% of the γH2Av foci in DAPI-bright are associated with TUNEL signal (TUNEL +) ($n > 50$). Graphs show mean ± SEM. Only Z-stacks including the DAPI-bright (dashed circles) are shown as projections in (A), (C) and (E). Scale bars = 1 μm.

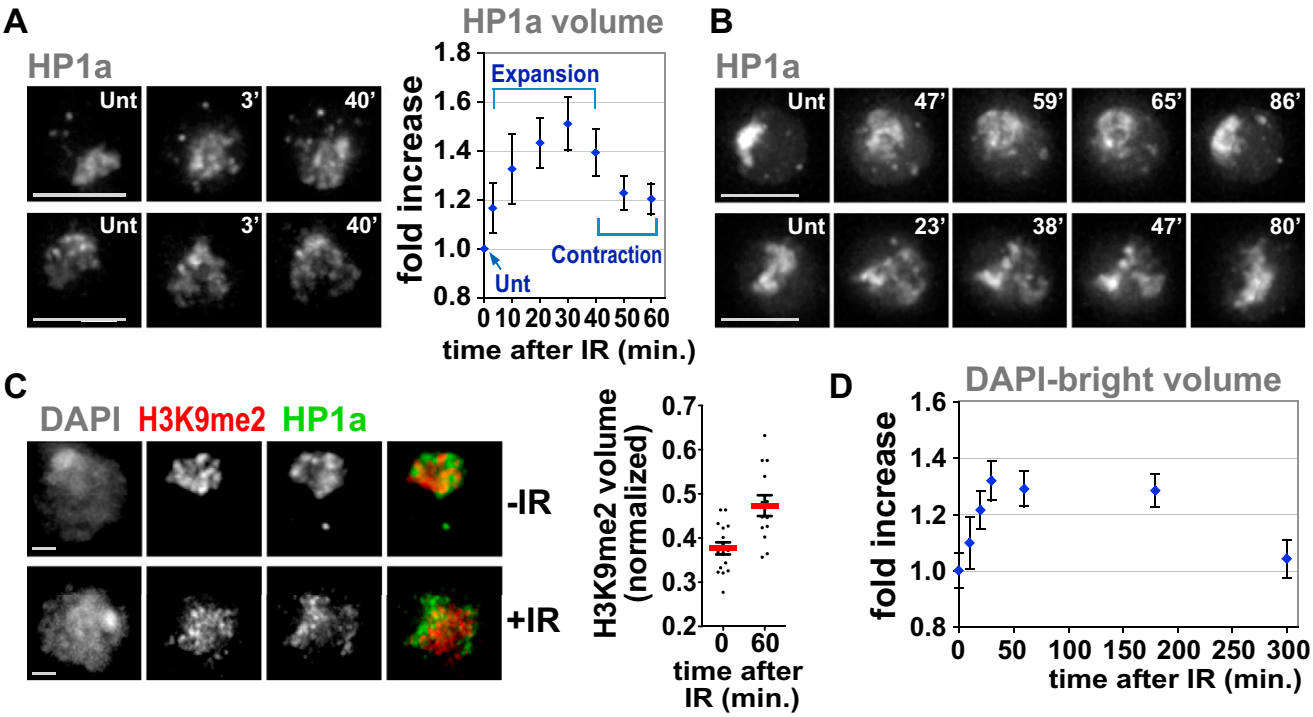


**Figure S3. Heterochromatin Expansion is an Early Response to IR, Related to Figure 2**

(A) Cells expressing mCh-HP1a were imaged before (Unt, time 0) and after IR. Left: images from significant time points are shown. Right: automated quantitation of 10 nuclei shows that expansion starts at 3 min after IR ($p < 0.01$, compared to 0 min/Unt), peaks at 20-40 min ($p < 0.0001$, compared to 0 min/Unt), and is followed by partial contraction ($p < 0.002$, compared to 20-40 min) (two-tailed t test). Scale bars = 5 μm.

(B) Images from the experiment described in Figure 2B show partial contraction of the HP1a domain at later time points after IR. Scale bars = 5 μm.

(C) Left: Images of H3K9me2, HP1a and DAPI IF from cells before (-) and 60 min after (+) IR. Right: quantitation of the volume occupied by H3K9me2 shows expansion after IR ($p < 0.005$ by two-tailed t test, $n > 15$). The H3K9me2 volume was quantified with softWoRX and normalized to the nuclear volume (DAPI). Scale bars = 1 μm.

(D) Cells were fixed before (time 0) and at different time points after IR. Automated quantitation of the DAPI-bright volume shows significative expansion at 30 min after IR (1.3 fold compared to untreated, $p < 0.001$, $n > 100$) and significant contraction by 5h (180 versus 300 min, $p < 0.05$, $n > 100$). Note that at 5 hr the DAPI-bright volume is not significantly different from untreated cells, indicating complete contraction to pre-IR volumes.

(E) ChIP-array analysis of HP1a before (Unt), 30 min and 60 min after IR. The browser view of chromosome 2 and arm 3L shows the position of the euchromatin-heterochromatin border (red line); *x* axis = genome coordinates in Mbs. *y* axis = enrichment p values, normalized to input for each time point. Purple rectangle = region shown in Figure 2C.

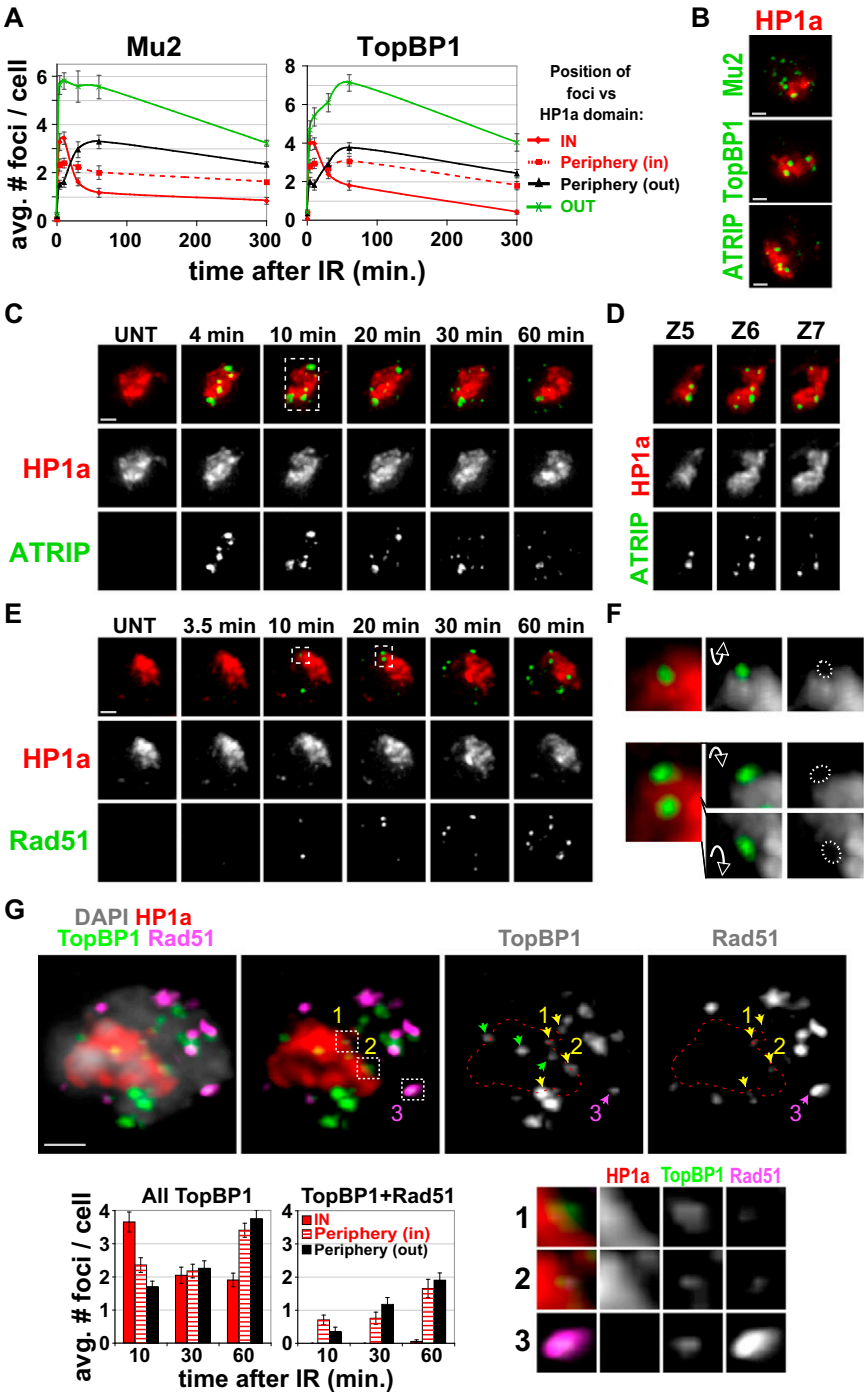


**Figure S4. Mu2, TopBP1, and ATRIP Foci Form Rapidly within the HP1a Domain after IR, whereas Rad51 Foci Only Form at the Periphery of the HP1a Domain, Related to Figure 3**

(A) Mu2 and TopBP1 foci are formed within the HP1a domain and then relocalize to its periphery. Cells expressing GFP-Mu2 and mCh-HP1a, or mCh-TopBP1 and GFP-HP1a, were imaged before and at different time points after IR. Top: Foci were classified as 'IN' when completely included within the HP1a domain, 'Periphery IN' when located along the inside edge of the HP1a domain, and 'Periphery OUT' when outside the HP1a domain but touching its surface. 'OUT' primarily contains foci that were completely external to HP1a, but also includes relocalizing foci connected to the heterochromatin by faint HP1a protrusions/filaments; since these connections can be difficult to visualize in HP1a volume modeling, inclusion in the OUT category provides the most conservative approach, even if it includes some foci that belong in the 'Periphery OUT' class. Mu2 and TopBP1 foci form within the HP1a domain (IN) by 4 min and decrease > 10 min after IR, similar to the kinetics observed for ATRIP foci (Figure 3A). Then they accumulate at the periphery of the HP1a domain between 10 and 60 min after IR

($p < 0.001$, $n = 30$). In euchromatin (OUT), Mu2 foci form at very early time points, similar to γH2Av foci in fixed samples (Figure 1B), whereas TopBP1 foci appear later, similar to the dynamics of ATRIP foci (Figure 3A).

(B) Images of cells expressing Mu2, TopBP1 or ATRIP at 6 min after IR show that Mu2 foci have similar intensity and uniform distribution in euchromatin and heterochromatin at early time points, whereas TopBP1 and ATRIP foci are much brighter and more abundant within the HP1a domain.

(C) ATRIP foci are formed within the HP1a domain. Stills from Movie S2 are shown where cells expressing GFP-ATRIP and mCh-HP1a were imaged before (UNT) and after IR. 4 and 10 min after IR, bright ATRIP foci are mostly localized within the HP1a domain (see D). Over time, they move to the periphery and outside the HP1a domain, and then become weaker.

(D) Analysis of individual Z-stacks was used to identify ATRIP foci localized within the HP1a domain (these examples are from the region indicated by the dashed box in (C).

(E) Rad51 foci only form at the periphery and outside the HP1a domain at late time points after IR. Cells expressing GFP-Rad51 and mCh-HP1a were imaged as in (C), and are shown as projections. Time points were selected to allow a direct comparison with ATRIP foci (C). Rad51 foci appear later than ATRIP foci and are localized only outside or at the periphery of HP1a.

(F) Rotation of the nuclei in 3D reconstructions shows local HP1a exclusion where Rad51 foci are formed. Three foci from the regions outlined in (E) are shown. Dashed circles = Rad51, arrows indicate direction of rotation relative to (E).

(G) Cells expressing mCh-TopBP1 (green) and GFP-HP1a (red) from the experiment described in (A) were fixed at different time points after IR and stained for Rad51 (pink) and DAPI (gray). An example of a cell fixed at 60 min after IR is shown (top). TopBP1 foci were classified based on their positions with respect to the HP1a domain as in (A) and scored for colocalization with Rad51 foci. Quantitation (bottom left) shows that the number and distribution of TopBP1 foci in fixed samples confirms observations from the time-lapse experiments (compare the graph on the left with A; only foci within and at the periphery of the HP1a domain are shown here). TopBP1 foci are not associated with Rad51 within the HP1a domain, and the frequency of colocalization with Rad51 foci progressively increases at the periphery of the HP1a domain ($p < 0.001$,'Periphery IN': 60 min versus 30 min, and Periphery 'OUT': 60 min versus 30 min, and 30 min versus 10 min; $n > 20$). Interestingly, most Rad51 foci observed at the periphery of the HP1a domain (examples 1 and 2 from the regions outlined) are much weaker than those observed outside the HP1a domain (example 3), which tend to associate with weaker TopBP1 foci. This observation is consistent with the expected progressive substitution of TopBP1by Rad51. Green arrows = examples of TopBP1 foci that do not overlap with Rad51; Yellow arrows = examples of TopBP1 foci that overlap with small Rad51 foci at the periphery of the HP1a domain; Pink arrow = example of a small TopBP1 signal that overlaps with a bright Rad51 focus outside the HPa domain.

Graphs show mean ± SEM. Scale bars = 1 μm.

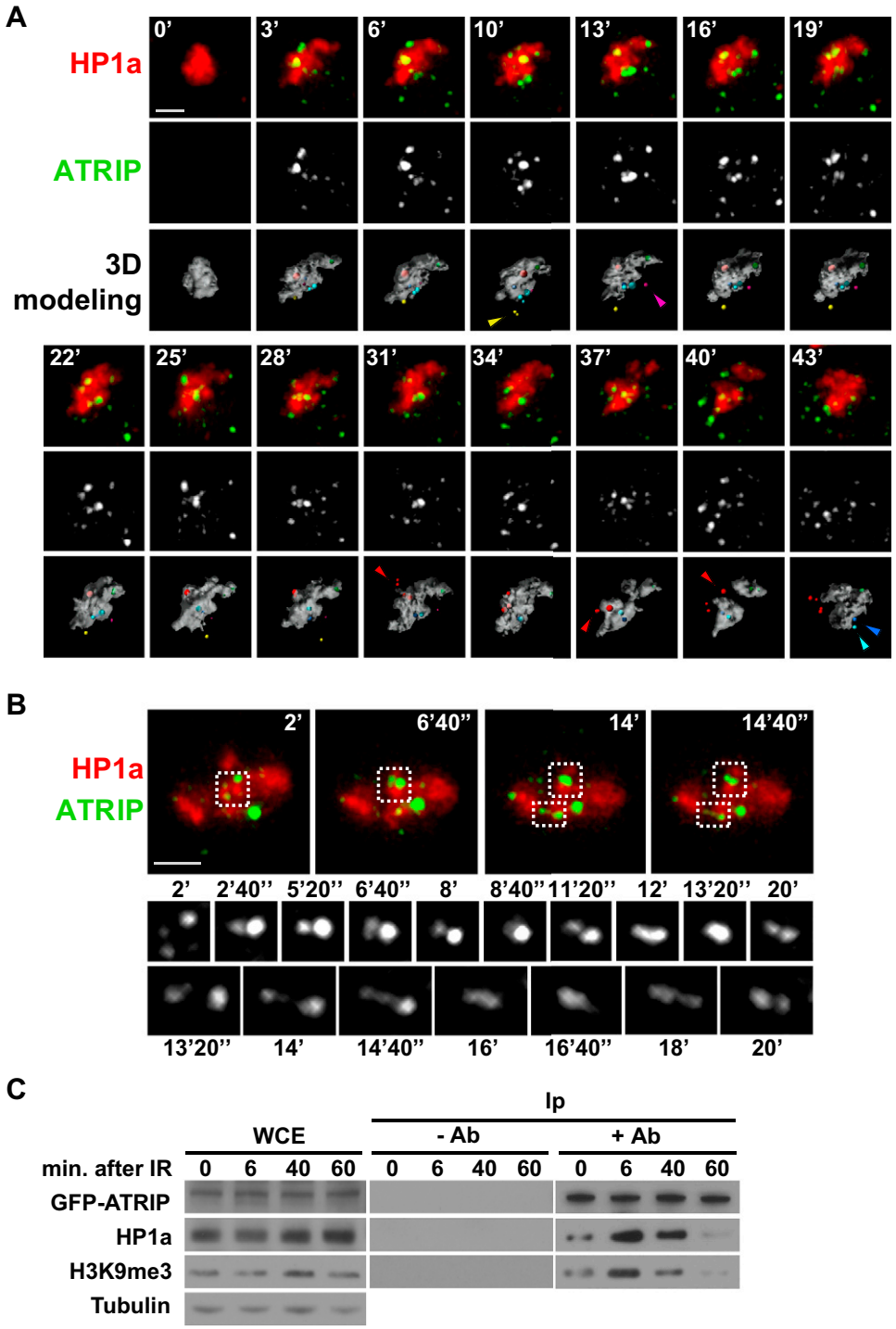


**Figure S5. ATRIP Foci Are Highly Dynamic within the HP1a Domain, Related to Figure 3**

(A) ATRIP foci relocalize at the periphery and outside the HP1a domain. Cells expressing GFP-ATRIP (green) and mCh-HP1a (red) were imaged before and every 3 min after IR. All the time points from Movie S3 are shown, which is another example of data shown in Figure 3A and Movie S2. 3D modeling (a subset of time points shown in Figure 3C) shows representative ATRIP foci formed within the HP1a domain that translocate outside at the indicated time points (arrows). ATRIP foci frequently split over time (see red, cyan, yellow foci). Scale bar = 1 μm.

(B) ATRIP foci split and fuse within the HP1a domain. Top: stills from Movie S4, where cells expressing GFP-ATRIP and mCh-HP1a were imaged every 40 s starting from 2 min after IR. Significant time points for the regions outlined are shown at the bottom. Scale bars = 1 μm.

(C) ATRIP physically interacts with heterochromatin components, and the level of association changes in response to IR. Kc cells expressing GFP-ATRIP were used to immunoprecipitate ATRIP in the absence (time 0) or at different time points after IR, with anti-GFP antibodies (+Ab). Western blot with anti-GFP, HP1a and H3K9me3 antibodies shows strong enrichment of HP1a and H3K9me3 at 6 and 40 min after IR compared to 0 min. Weaker enrichments at 0 and 60 min were also observed in comparison with a control Ip performed on the same extracts in the absence of antibody (-Ab). Tubulin is the loading control. Thus, some ATRIP interacts directly or indirectly with heterochromatin components before damage induction, but the recovery is significantly higher 6 min after IR when bright ATRIP foci are located within the HP1a domain. The recovery of HP1a and H3K9me3 is slightly reduced at 40 min when many ATRIP foci have relocated to the HP1a periphery/outside the domain, and returns to pre-IR levels (or below) by 60 min, when relocalization is complete and most ATRIP foci are outside the HP1a domain.

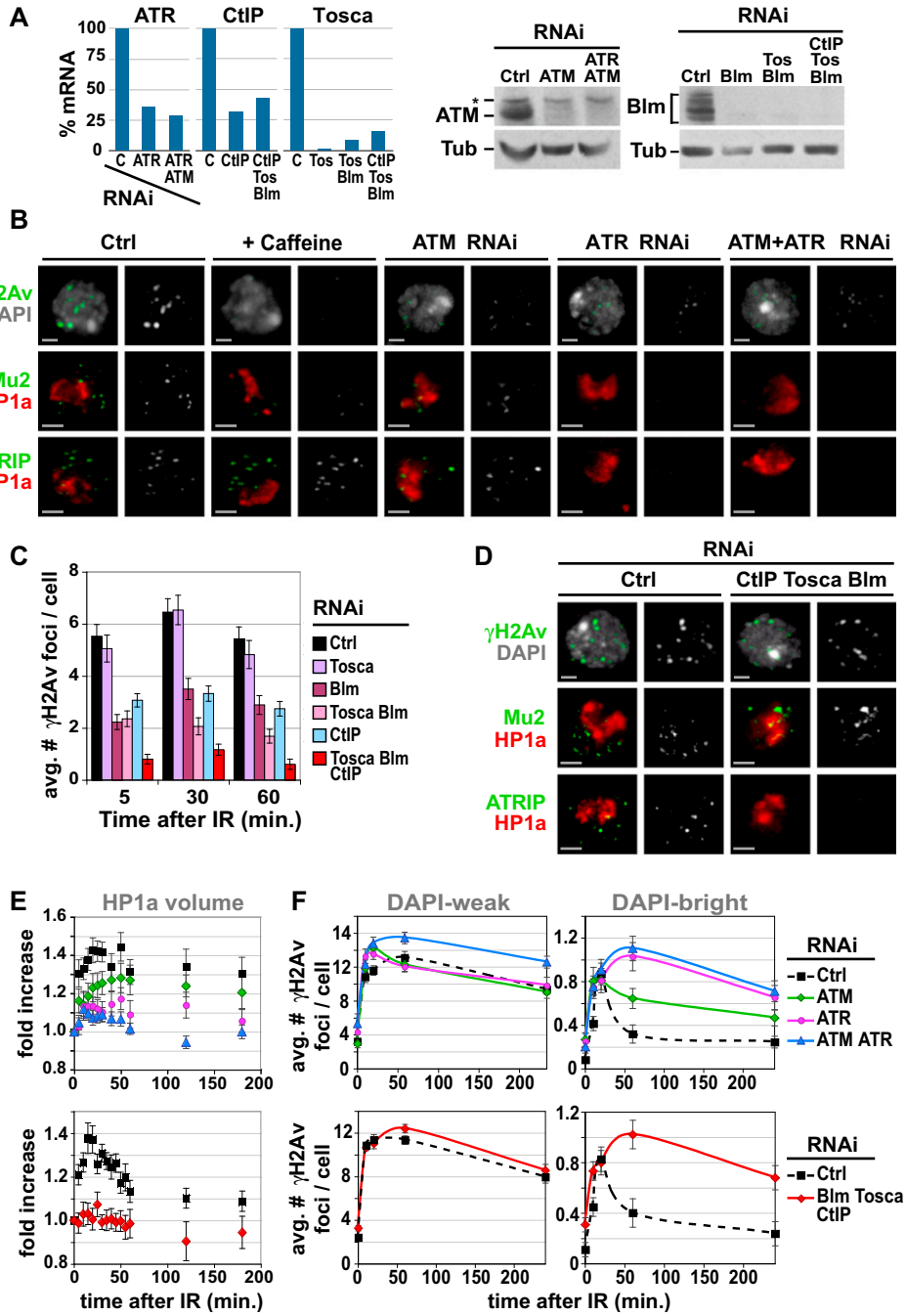


**Figure S6. Impact of Checkpoint and Resection Inactivation on the DSB Response, Related to Figure 4**

(A) Cells from the experiments described in Figures 4E, S6B, S6D and S6F were analyzed by Q-PCR (left), which confirm significant reduction in ATR CtIP, Tosca (Tos) mRNA levels, compared to control RNAi. Western analyses confirm ATM and Blm protein depletion after RNAi (right). Tubulin (Tub) is used as loading control and (*) is a non-specific band.

(B) Inactivation of the checkpoint by caffeine or RNAi results in defective DNA damage response. Cells were treated with caffeine, or ATM and/or ATR were depleted by RNAi. Top row: IF analysis of cells fixed at 10 min after IR show lower intensities of γH2Av foci compared to cells that were not treated with caffeine (Ctrl in B), or cells treated with Ctrl RNAi (Ctrl in D), although the total number of foci did not change significantly (quantitation in F, 10 min). Middle row: Imaging of cells expressing GFP-Mu2 and mCh-HP1a at 60 min after IR show that the intensity of Mu2 foci is not affected by ATM RNAi, but is defective after caffeine treatment, and ATR or ATR + ATM depletion. The number of GFP-Mu2 foci is not affected by ATM RNAi, but significantly decrease after caffeine treatment (1.5-fold decrease compared to control), ATR or ATR + ATM RNAi (2.5 and 2.6-fold decrease, respectively) ($p < 0.01$, $n > 50$). These results suggest that ATR plays a critical role in the formation of Mu2 foci in *Drosophila*. Bottom row: Imaging of cells expressing GFP-ATRIP and mCh-HP1a at 60 min after IR shows no overall defects in the number and intensity of ATRIP foci after ATM depletion. Conversely, ATR and ATR + ATM RNAi almost completely abolished formation of ATRIP

foci. The strong defect after ATR RNAi could result from instability of ATRIP in the absence of ATR, as previously shown in mammalian cells (Cortez et al., 2001). In contrast, intensities of ATRIP foci were not affected when ATR kinase activity was inactivated with caffeine (described in Figure 4A). These results suggest that the ATR kinase activity is not required for ATRIP recruitment to RPA-covered resected DNA.

(C) Depletion of resection proteins by RNAi results in defective ATRIP foci in response to IR. Tosca, Blm and/or CtIP were depleted in cells expressing GFP-ATRIP and mCh-HP1a, and cells were imaged at different time points after IR. Quantitation shows that the number of ATRIP foci decreases about 2-fold after depletion of Blm or CtIP, 3-fold after depletion of Blm + Tosca, and 7-fold after depletion of Blm + Tosca + CtIP, compared to control RNAi. Although depletion of Tosca alone does not impair the formation of ATRIP foci, depletion of Blm + Tosca results in lower ATRIP foci compared to Blm RNAi alone, suggesting independent functions of Blm and Tosca in resection ($p < 0.01$ for all the comparisons, $n > 100$). Values were normalized to the number of ATRIP foci in untreated cells.

(D) Resection is impaired by Tosca, Blm and CtIP RNAi depletion. IF analysis of cells fixed at 10 min after IR shows no defects in γH2Av foci formation (top) compared to control RNAi. Cells expressing GFP-Mu2 and mCh-HP1a (middle) or GFP-ATRIP and mCh-HP1a (bottom) at 60 min after IR show defective assembly of ATRIP foci and no defects in Mu2 foci compared to control RNAi. The absence of effects of RNAi depletion on γH2Av and Mu2 foci (which bind DSBs before resection), coupled with the absence of ATRIP foci (ATRIP recruitment requires RPA-covered ssDNA), strongly suggests defects in resection, but not prior processing of DSBs (Sartori et al., 2007).

(E and F) Checkpoint proteins and resection are required for heterochromatin expansion and relocalization of foci in response to IR. All the time points for the analyses described in Figure 4D and 4E are shown. ATM, ATR, or ATM + ATR RNAi results in defective HP1a expansion (E, top) and persistent γH2Av foci in DAPI-bright (F, top) after IR. Quantitation shows that ATR + ATM RNAi results in increased γH2Av foci also in euchromatin (DAPI-weak) compared to control RNAi ($p < 0.01$, $n > 100$). Blm + Tosca + CtIP RNAi results in defective HP1a expansion (E, bottom) and persistent γH2Av foci in DAPI-bright (but not in DAPI weak) (F, bottom) after IR.

Graphs show mean ± SEM. Images are maximum intensity projections. Scale bars = 1μm.

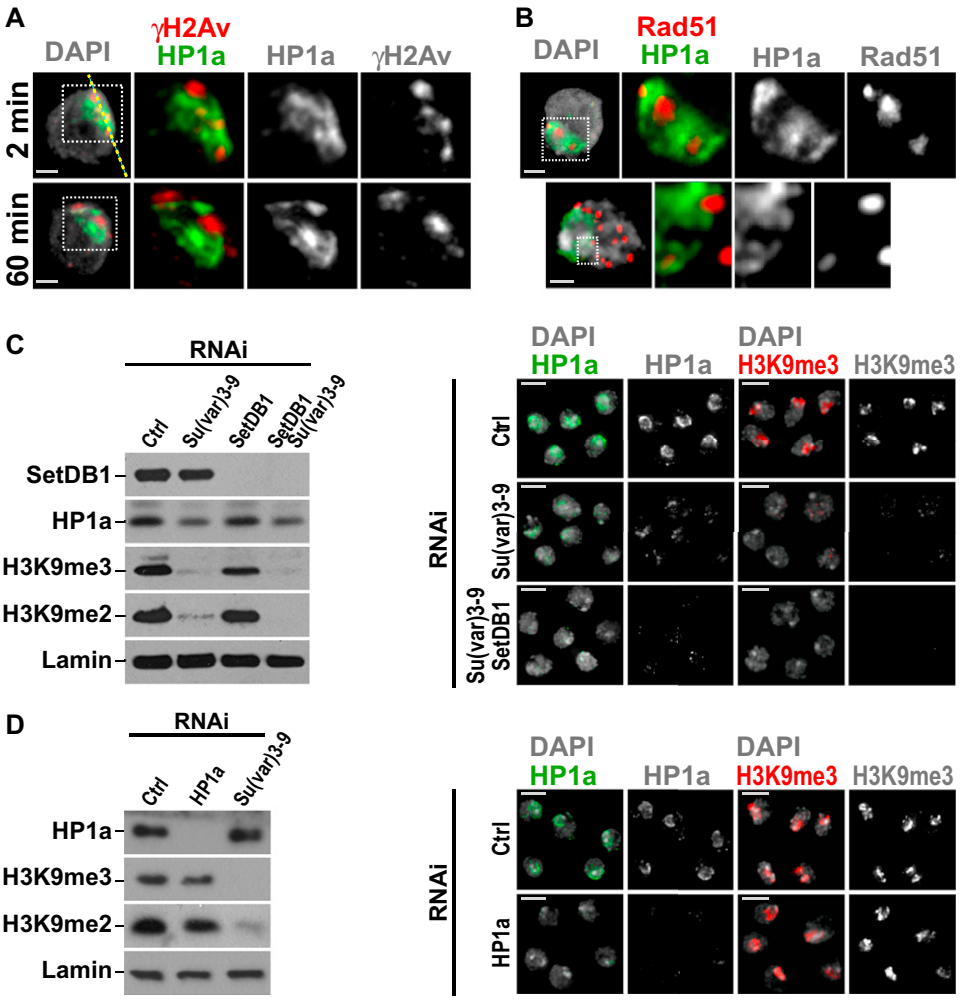


**Figure S7. Su(var)3–9 and SetDB1 Depletion, and Not HP1a Depletion, Result in Loss of H3K9me2 and me3 in Heterochromatin, Related to Figure 5**

(A) γH2Av foci are associated with the HP1a domain minutes after NIR treatment but not at later time points. Immunodetection of γH2Av (red) and HP1a (green) in cells fixed after NIR laser treatment (position shown by yellow dashed line) shows that γH2Av signals overlap with the HP1a domain at 2 min but not at 60 min after IR. Dashed squares indicate the regions zoomed on the right. Images are individual Z stacks. Scale bars = 1 μm. Formation of γH2Av foci within the HP1a domain at early time points after NIR treatment, and reciprocal exclusion between γH2Av and HP1a at later time points, mirrors what is observed in response to IR (γH2Av associated to the DAPI-bright domain at 10 min and not at 60 min, Figure 1A and 1B). This suggests that different sources of DSBs trigger similar responses in heterochromatin.

(B) HP1a and Rad51 recruitment to DSBs are mutually exclusive. Immunodetection of Rad51 (red) and HP1a (green) in cells fixed 60 min after NIR laser treatment (top) or IR (bottom) shows that Rad51 foci are formed in regions that lack HP1a signal. Top: The image shows a single Z stacks. Bottom: The image is a maximum intensity projection of multiple Z stacks including the HP1a domain. Scale bars = 1 μm.

(C) Western analysis (left) and IF (right) of cells from the experiment in Figure 5A confirm that RNAi of Su(var)3-9 or Su(var)3-9 and SetDB1 result in significant protein depletion, and loss of H3K9me2, H3K9me3 and HP1a at heterochromatin. HP1a is visible only at telomeric loci after depletion of both HMTases (right and data not shown), consistent with previous analyses demonstrating that HP1a telomeric binding is independent of H3K9 methylation (Perrini et al., 2004).

(D) Western analysis (left) and IF (right) of cells from the experiments in Figure 5B show that HP1a RNAi results in complete HP1a depletion, but has minimal effects on H3K9me2 and H3K9me3 levels. Su(var)3-9 RNAi, which does significantly reduce H3K9me2 and H3K9me3 levels is shown for comparison. Lamin = loading control. Scale bars = 5 μm. Images are maximum intensity projections.

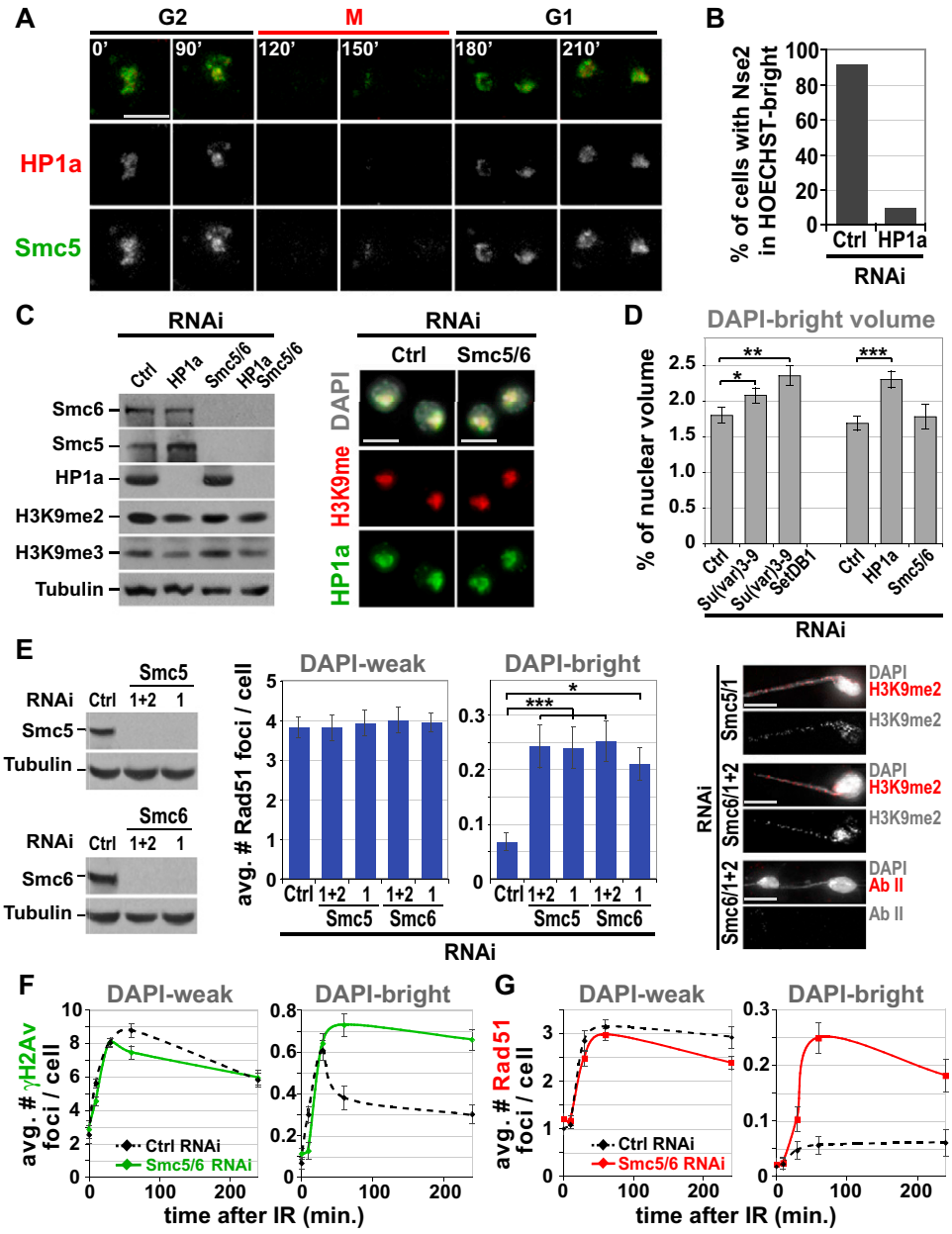


**Figure S8. Depletion of the Smc5/6 Complex Results in an Abnormal DSB Response in Heterochromatin, Related to Figure 6**

(A) The Smc5/6 complex and HP1a are disassembled from heterochromatin in mitosis and reassembled in G1. Cells expressing GFP-Smc5 and mCh-HP1a were imaged as in Figure S1D and shown as projections. Both HP1a and Smc5 signals become diffuse in mitosis, then Smc5 relocalizes to the HP1a domain that forms in G1.

(B) HP1a is required for localization of the Smc5/6 complex to heterochromatin. Quantitation of the experiment shown in Figure 6C shows that HP1a depletion by RNAi results in delocalization of GFP-Nse2 from HOECHST-bright heterochromatin ($p < 0.0001$ by Fisher's exact test, $n > 100$). HOECHST (0.5 μg/ml) was added to the culture 5 min before imaging. Since HOECHST might potentially introduce DNA breaks, we verified that these conditions did not induce formation of ATRIP foci in cells expressing GFP-ATRIP and mCh-HP1a (data not shown). The use of HOECHST as a marker for heterochromatin was confirmed by colocalization with mCh-HP1a (data not shown).

(C) Left: Western analysis of cell extracts prepared from the experiment in Figure 6D confirms that RNAi of Smc5, Smc6 and HP1a for 5 days results in depletion of the target proteins. Smc5/6 RNAi doesn't reduce the levels of H3K9me2, H3K9me3 and HP1a, and HP1a depletion does not reduce overall levels of Smc5 and 6. Right: IF with anti-H3K9me2, anti-H3K9me3 (assayed simultaneously) and HP1a shows that the distribution of heterochromatin markers also doesn't change after Smc5/6 RNAi. These results, combined with mislocalization of Nse2 after HP1a depletion (B), demonstrate that localization of the Smc5/6 complex to heterochromatin requires HP1a, whereas normal levels and localization of H3K9 methylation and HP1a do not require Smc5/6.

(D) Automated quantitation of the DAPI-bright volume in cells fixed after Su(var)3-9, Su(var)3-9 + SetDB1 or HP1a show expansion of DAPI-bright compared to control RNAi (*p = 0.05, **p < 0.05, ***p < 0.001) (one-tailed Mann-Whitney test, n > 100), and further expansion after IR (not shown). Smc5/6 RNAi does not result in DAPI-bright expansion, consistent with data showing that Smc5/6 is not required for heterochromatin formation (C).
(E) Depletion of either Smc5 or Smc6 promotes abnormal recombination in heterochromatin. Depletion of Smc5 or Smc6 individually with different dsRNAs was confirmed by Western analysis (left). After 5 days of RNAi, there is a significant increase in the frequency of Rad51 foci in DAPI-bright (and not in DAPI-weak) at 60 min after IR (center) (***p < 0.001, *p < 0.01, n > 150). After 6.5 days of RNAi, cells were processed as in Figure 6F and DNA fibers connecting mitotic cells appear (right), as observed after simultaneous depletion of both Smc5 and Smc6 (Figure 6E). Immunodetection of H3K9me2 shows enrichment of heterochromatin marks along the fibers (right), compared with a control stained with only secondary antibodies (Ab II).
(F and G) Smc5/6 depletion results in persistent γH2Av foci and abnormal formation of Rad51 foci in DAPI-bright. Smc5 and Smc6 were depleted for 5 days by RNAi, then cells were fixed at different time points after IR and stained for γH2Av or Rad51 and DAPI. Quantitation of γH2Av foci (F) after Smc5/6 depletion shows a significant increase in DAPI-bright (and not in DAPI-weak) at 60 and 240 min after IR, compared to control RNAi (p < 0.01, n > 100). Rad51 foci (G) increase significantly in DAPI-bright (and not in DAPI-weak) after Smc5/6 depletion at 60 and 240 min after IR, compared to control RNAi (p < 0.001, n > 150).
Scale bars = 5 μm. Images are maximum intensity projections. Graphs show mean ± SEM.